Tunable and enhanced simultaneous photoluminescence–electricity–magnetism trifunctionality successfully realized in flexible Janus nanofiber

Duanduan Yin · Qianli Ma · Xiangting Dong ·
Nan Lv · Jinxian Wang · Wensheng Yu ·
Guixia Liu

Abstract YF_3:Eu^{3+} nanofibers, polyaniline (PANI) and ferroferric oxide (Fe_3O_4) nanoparticles (NPs) were incorporated into polyvinyl pyrrolidone (PVP) and electrospun into Janus nanofibers with YF_3:Eu^{3+} nanofibers/PVP as one half side and PANI/Fe_3O_4/PVP as the other half side. The morphology and properties of the final products were investigated in detail by X-ray diffractometry, scanning electron microscopy, transmission electron microscopy, energy dispersive spectrometry, Hall effect measurement system, fluorescence spectroscopy, vibrating sample magnetometry and UV–Vis spectroscopy. The results reveal that the [YF_3:Eu^{3+}/PVP]//[PANI/Fe_3O_4/PVP] trifunctional Janus nanofibers possess excellent electrical conduction, magnetism and fluorescence due to their peculiar isolated nanostructure. Fluorescence emission peaks of Eu^{3+} are observed in the [YF_3:Eu^{3+}/PVP]//[PANI/Fe_3O_4/PVP] Janus nanofibers and assigned to the $^5D_0 \rightarrow {}^7F_1$ (587, 595 nm), $^5D_0 \rightarrow {}^7F_2$ (614, 622 nm), and the $^5D_0 \rightarrow {}^7F_1$ magnetic-dipole transition at 595 nm is the predominant emission peak. The electrical conductivity reaches up to the order of 10^{-4} S cm^{-1}. The luminescent intensity, electrical conductivity and saturation magnetization of the Janus nanofibers can be respectively tunable by adjusting respective amounts of YF_3:Eu^{3+} nanofibers, PANI and Fe_3O_4 NPs. The new type trifunctional Janus nanofibers have many potential applications in the fields of electromagnetic interference

shielding, microwave absorption, molecular electronics and biomedicine. More importantly, this design concept and construct technology is of universal significance to fabricate other multifunctional nanostructures.

1 Introduction

Electrospinning is an outstanding technique to process viscous solutions or melts into continuous fibers with diameters ranging from micrometer to submicron or nanometer. This method not only attracts extensive academic investigations [1–9], but is also applied in many fields such as filtration [10], nanocables [11], optical and chemical sensors [12], electrode materials [13], and biological scaffolds [14].

Conducting polymers, for instance, polyaniline (PANI), polypyrrole and polythiophene, PANI is found to be the most promising conducting polymer because of its high conductivity, ease of synthesis, processibility, environmental stability, and wide applications compared to other intrinsically conducting polymers. The order of conductivity of PANI is higher than that of common polymers ($<10^{-9}$ S cm^{-1}), but lower than that of typical metals ($>10^4$ S cm^{-1}). PVP has been widely used for electrospinning owing to its good solubility, high flexibility, nontoxicity, easy obtainment, low costs, etc. More importantly, it has been found that a new typed hybrid polymer with both excellent conductivity and spinnability can be achieved by mixing PVP and PANI together [9, 15]. Fe_3O_4 NPs have attracted a lot of interest of scientists recently due to their wide applications, such as biomacromolecule separation, catalyst separation, drug/gene delivery and release, and magnetic resonance imaging [16, 17]. YF_3 is one of the most important matrixes for lanthanide-doped phosphors,

D. Yin · Q. Ma · X. Dong (✉) · N. Lv · J. Wang ·
W. Yu (✉) · G. Liu
Key Laboratory of Applied Chemistry and Nanotechnology at Universities of Jilin Province, Changchun University of Science and Technology, Changchun 130022, China
e-mail: dongxiangting888@163.com

W. Yu
e-mail: wenshengyu2009@sina.com

providing a wide band gap (>10 eV) and suitable Y^{3+} sites where Y^{3+} can be easily substituted by other trivalent rare earth ions without additional charge compensation [18]. YF_3:Eu^{3+} nanomaterials have wide and potential applications in optical devices. These outstanding luminescent characteristics are attributed to sharp absorption and emission bands of the doped Eu^{3+} ions in the ultraviolet, visible and infrared wavelength regions, which originate from f–d and f–f transitions of Eu^{3+} ions.

Currently, multifunctional nanomaterials have attracted much attention of scientists and investigation on the luminescent–electrical–magnetic twi- or tri-functional nanomaterials has become a hot topic of research in the field of nanomaterials [19, 20]. Magnetic–photoluminescent bifunctional nanomaterials have been applied in medical diagnostics and optical imaging, etc. [21, 22]. Our group has prepared Fe_3O_4/PVP@Eu(BA)$_3$phen/PVP coaxial nanocables [23] and [Fe_3O_4/PVP]//[Eu(BA)$_3$phen/PVP] bistrand-aligned composite nanofibers bundles [24] via electrospinning. Electromagnetically functionalized micro/nanostructures of conducting polymers are of special interest due to their potential applications in electrochromic device, electromagnetic interference shielding, non-linear optical systems, biomedicine and microwave absorbers [25–27]. Meng et al. [28] have synthesized core–shell structure Fe_3O_4@C@polyaniline magnetic microspheres by using simple hydrothermal reactions. Wan et al. [29, 30] studied a series of PANI composites containing Fe_3O_4 nanomagnets prepared by chemical polymerization. Deng et al. [31] reported the preparation of PANI/Fe_3O_4 nanoparticles with core–shell structure via an in situ polymerization of aniline monomer in an aqueous solution, which contained Fe_3O_4 nanoparticles and surfactant. Xuan et al. [32] synthesized superparamagnetic Fe_3O_4/polyaniline core/shell microspheres with well-defined blackberry-like morphology via a simple in situ surface polymerization method. Very recently, the preparation of Fe_2O_3/Eu(DBM)$_3$(bath)/PVP composite nanofibers [33], Fe_3O_4/Eu(BA)$_3$phen/PVP composite nanofibers [34] and PANI particles/rare earth complex/PVP composite nanofibers [35, 36] via electrospinning was emerged. From above studies, it is found that the existence of PANI particles and Fe_3O_4 will greatly decrease the luminescent intensity of rare earth compounds if PANI particles or Fe_3O_4 nanoparticles contact directly with the rare earth luminescent compounds, and the nanofibers have poor electrical conduction due to the fact that PANI particles were not mutually connected in the nanofibers and space among PANI particles was existed.

In order to achieve high conductivity and strong luminescence, PANI must have good consecutiveness in the nanofibers leading to more effective electrons transport, while luminescent materials must be effectively separated from electrical and magnetic materials. In the procedure of seeking a way to realize this academic idea, we were inspired by the reports on the Janus nanomaterials [37–43]. 'Janus' is the name of an ancient Roman God, who has two faces peering into the past and the future. Named after this Roman God, Janus particles have two distinguished surfaces/chemistries on the two sides. Pierre-Gilles de Gennes, Nobel Prize in Physics winner, made the Janus particles known to the scientific community. Upon the unique feature of the asymmetry dual-sided Janus structure, in this paper, we employ electrospinning technique using specially designed parallel spinnerets to prepare [YF_3:Eu^{3+}/PVP]//[PANI/Fe_3O_4/PVP] luminescent–electrical–magnetic trifunctional Janus nanofibers with YF_3:Eu^{3+} nanofibers/PVP as one half side and PANI/Fe_3O_4/PVP as the other half side. The conductivity, magnetism and photoluminescence of Janus nanofibers were studied through comparing with YF_3:Eu^{3+}/PANI/Fe_3O_4/PVP composite nanofibers.

2 Experimental sections

2.1 Chemicals

Polyvinyl pyrrolidone (PVP, Mw $\approx$ 90,000), Y_2O_3 (99.99 %), Eu_2O_3 (99.99 %), HNO_3, and dimethylformamide (DMF) were bought from Tianjin Tiantai Fine Chemical Co., Ltd. Anhydrous ethanol, aniline, $FeCl_3 \cdot 6H_2O$, NH_4HF_2, $FeSO_4 \cdot 7H_2O$, NH_4NO_3, polyethyleneglycol (PEG, Mw $\approx$ 20,000), ammonia and (IS)-(+)-Camphor-10 sulfonic acid (CSA) were bought from Sinopharm Chemical Reagent Co., Ltd. Ammonium persulfate were purchased from Guangdong Xilong Chemical Co., Ltd. All the reagents were of analytical grade and directly used as received without further purification. Deionized water was homemade.

2.2 Synthesis of Fe_3O_4 nanoparticles

Fe_3O_4 NPs were obtained via a facile coprecipitation synthetic method and PEG was used as the protective agent to prevent the particles from aggregating. One typical synthetic procedure was as follows: 5.406 g of $FeCl_3 \cdot 6H_2O$, 2.78 g of $FeSO_4 \cdot 7H_2O$, 4.04 g of NH_4NO_3 and 1.9 g of PEG were added into 100 mL of deionized water to form uniform solution under vigorous stirring at 50 °C. To prevent the oxidation of Fe^{2+}, the reactive mixture was kept under argon atmosphere. After the mixture had been bubbled with argon for 30 min, 0.1 mol/L of $NH_3 \cdot H_2O$ was dropwise added into the mixture to adjust the pH value above 11. Then the system was continuously bubbled with argon for 20 min at 50 °C, and black precipitates were

formed. The precipitates were collected from the solution by magnetic separation, washed for three times with deionized water, and then dried in an electric vacuum oven at 60 °C for 12 h.

2.3 Preparation of $YF_3:Eu^{3+}$ nanofibers

Taking YF_3:5 %Eu^{3+}[5 % stands for molar percentage of Eu^{3+} to $(Y^{3+}+Eu^{3+})$] nanofibers as an example to prepare $YF_3:Eu^{3+}$ nanofibers, $YF_3:Eu^{3+}$ nanofibers were fabricated via monoaxial electrospinning combined with double-cruci-ble fluorination technique [44]. The detailed procedure was as follows: 2.4 g of rare earth nitrate, including $Y(NO_3)_3 \cdot 6H_2O$ and $Eu(NO_3)_3 \cdot 6H_2O$, was dissolved in 21.8667 g of DMF, and then 2.4 g of PVP was added into the above solution under magnetic stirring for 8 h to form homogeneous trans-parent spinning solution. The spinning solution was electro-spun at room temperature under a positive high voltage of 14 kV, the distance between the spinneret tip and the collector (Aluminum foil) was fixed to 15 cm, and air relative humidity was 50–70 %. With the evaporation of DMF, a dense web of PVP/$[Y(NO_3)_3 + Eu(NO_3)_3]$ composite nanofibers were formed on the collector. The above composite nanofibers were calcined at a heating rate of 1 °C min^{-1} and remained for 8 h at 700 °C. Thus, $Y_2O_3:Eu^{3+}$ nanofibers were obtained. $Y_2O_3:Eu^{3+}$ nanofibers were loaded into a small crucible, and a few carbon rods were put into a big crucible, then the small crucible was placed into the big crucible. Next, some NH_4HF_2 powders were loaded into the space between the two crucibles, and then the big crucible was covered with its lid. This process is called double-crucible method. Finally

the crucibles were annealed at 280 °C for 2 h, then heated to 450 °C and remained for 3 h with the heating rate of 2 °C min^{-1}, then the temperature was decreased to 200 °C at a rate of 1 °C min^{-1} followed by natural cooling down to ambient temperature. Thus, $YF_3:Eu^{3+}$ nanofibers were acquired.

2.4 Fabrication of luminescent–electrical–magnetic trifunctional Janus nanofibers via electrospinning

In the preparation of the spinning solutions, aniline was dissolved in DMF with magnetic stirring at room temper-ature, and then PVP and CSA were slowly added into the above solution with magnetic agitation for 2 h. The mix-ture was then cooled down to 0 °C in an ice-bath for 1 h. The mixture was denoted as solution I. A mixed solution of ammonium persulfate (APS) and 2.000 g of DMF at 0 °C was prepared as the solution II. The solution II was added dropwise into the solution I under magnetic stirring. The final mixture was allowed to react at 0 °C for 24 h and then Fe_3O_4 were added into the mixture under magnetic stirring for 24 h at room temperature, thus the spinning solution A was prepared, which was applied to prepare the strand PANI/Fe_3O_4/PVP nanofibers. Meanwhile, $YF_3:Eu^{3+}$ nanofibers were ultrasonically dispersed in DMF for about 10 min, then PVP was slowly added into the above mixture with magnetic agitation for 24 h at room temperature,thus the spinning solution B was obtained, which was used to fabricate the other strand $YF_3:Eu^{3+}$/PVP nanofibers. The compositions and contents of these spinning solutions were listed in Table 1.

Table 1 Compositions of spinning solutions for preparing [$YF_3:Eu^{3+}$/PVP]//[PANI/Fe_3O_4/PVP] Janus nanofibers

Samples	Spinning solutions	PVP (g)	DMF (g)	CSA (g)	APS (g)	PANI (g)	Fe_3O_4 (g)	$YF_3:Eu^{3+}$nanofibers (g)
S_1	A1	0.9000	4.1000	0.2245	0.4411	0.1800	0.3000	
	B1	0.9000	4.7250					0.9000
S_2	A2	0.9000	4.3940	0.3369	0.6615	0.2700	0.3000	
	B1	0.9000	4.7250					0.9000
S_3	A3	0.9000	4.7250	0.4490	0.8822	0.3600	0.3000	
	B1	0.9000	4.7250					0.9000
S_4	A4	0.9000	5.1000	0.7861	1.5435	0.6300	0.3000	
	B1	0.9000	4.7250					0.9000
S_5	A5	0.9000	4.3940	0.3369	0.6615	0.2700	0.4500	
	B1	0.9000	4.7250					0.9000
S_6	A6	0.9000	4.3940	0.3369	0.6615	0.2700	0.9000	
	B1	0.9000	4.7250					0.9000
S_7	A2	0.9000	4.3940	0.3369	0.6615	0.2700	0.3000	
	B2	0.9000	4.7250					1.3500
S_8	A2	0.9000	4.3940	0.3369	0.6615	0.2700	0.3000	
	B3	0.9000	4.7250					1.8000

Fig. 1 Schematic diagram of the electrospinning setup
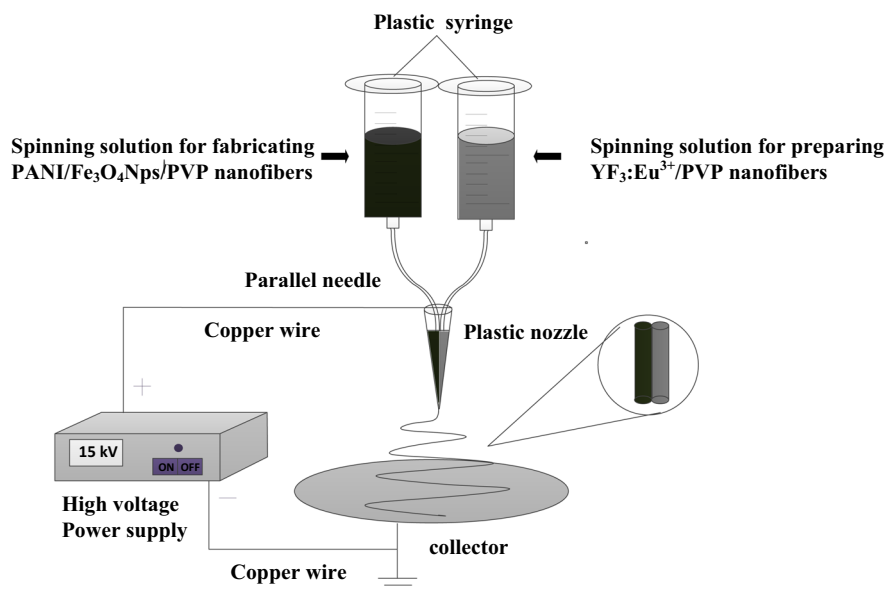
The specially designed parallel spinneret was used in this study and the electrospinning setup was indicated in Fig. 1. It is composed of a pair of stainless steel needles assembled side by side and fixed by a plastic nozzle. The two kinds of spinning solutions could have formed a side-by-side structure before they flow to the tip of the plastic nozzle. The spinning solutions A and B were respectively loaded into each plastic syringe. A piece of flat iron net was put about 15 cm away from the tip of the plastic nozzle as the nanofiber collector. A positive direct current (DC) voltage of 15 kV was applied between the spinneret and the collector to generate stable, continuous PVP-based Janus nanofibers at ambient temperature of 20–25 °C, and the air relative humidity of 28–32 %.

2.5 Fabrication of YF_3:Eu^{3+}/PANI/Fe_3O_4/PVP composite nanofibers

For comparison, YF_3:Eu^{3+}/PANI/Fe_3O_4/PVP composite nanofibers were also fabricated by mixing the spinning solution A2 and the spinning solution B1 together at the volume ratio of 1:1 and electrospun via the traditional single-spinneret electrospinning method. The spinning voltage, distance between the collector and the spinneret and other processing parameters were the same as those in the fabrication of the [YF_3:Eu^{3+}/PVP]//[PANI/Fe_3O_4/PVP] Janus nanofibers.

2.6 Characterization methods

The as-prepared Fe_3O_4 NPs, YF_3:Eu^{3+} nanofibers and [YF_3:Eu^{3+}/PVP]//[PANI/Fe_3O_4/PVP] Janus nanofibers were identified by an X-ray powder diffractometer (XRD, Bruker, D8 FOCUS) with Cu Kα radiation. The

morphology and internal structure of Janus nanofibers were observed by a field emission scanning electron microscope (FESEM, XL-30) and a transmission electron microscope (TEM, JEM-2010), respectively. The fluorescent properties of the samples were investigated by using a Hitachi fluorescence spectrophotometer F-7000. The elementary compositions of Janus nanofibers were determined by an energy dispersive X-ray spectrometer (EDS, GENESIE 2000). The conductivity property and the magnetic performance of samples were measured by Hall effect measurement system (ECOPIA HMS-3000) and a vibrating sample magnetometer (VSM, MPMS SQUID XL), respectively. The ultraviolet–visible spectra of samples were determined by a UV-1240 ultraviolet–visible spectrophotometer. All measurements were performed at room temperature.

3 Results and discussion

3.1 XRD analysis

The phase compositions of the Fe_3O_4 nanoparticles, YF_3:Eu^{3+} nanofibers and [YF_3:Eu^{3+}/PVP]//[PANI/Fe_3O_4/PVP] Janus nanofibers were identified by means of XRD analysis, as shown in Fig. 2. It can be seen from Fig. 2a that XRD patterns are conformed to the cubic structure of Fe_3O_4 (PDF#74-0748), and no characteristic peaks are observed for other impurities such as Fe_2O_3, FeO(OH). Figure 2b reveals the XRD patterns of YF_3:Eu^{3+} nanofibers, the diffraction peaks can be easily indexed to those of the pure orthorhombic phase with primitive structure of YF_3 (PDF#70-1935), and the space group is Pnma. No peaks of any other phases or impurities are also detected. As seen from the Fig. 2c, the XRD analysis result of
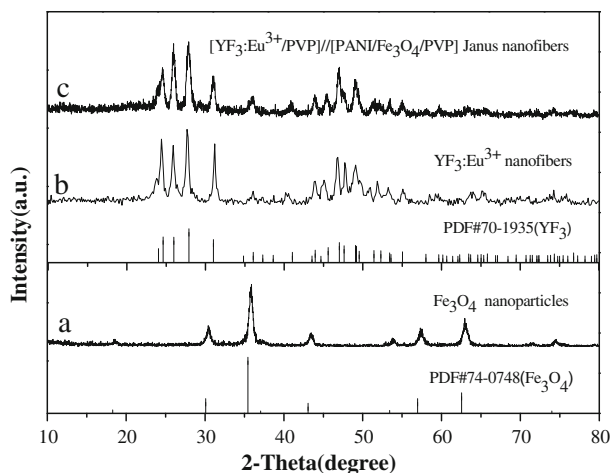
Fig. 2 XRD patterns of Fe_3O_4 nanoparticles (*a*), $YF_3:Eu^{3+}$ nanofibers (*b*) and $[YF_3:Eu^{3+}/PVP]//[PANI/Fe_3O_4/PVP]$ Janus nanofibers (*c*)

$[YF_3:Eu^{3+}/PVP]//[PANI/Fe_3O_4/PVP]$ Janus nanofibers demonstrates that the Janus nanofibers contain crystalline Fe_3O_4 nanoparticles and $YF_3:Eu^{3+}$.

3.2 Morphology and structure

Figure 3a, b show SEM images of the Fe_3O_4 nanoparticles and $YF_3:Eu^{3+}$ nanofibers. The diameter of the Fe_3O_4 NPs is 8–10 nm. The $YF_3:Eu^{3+}$ nanofibers have smooth surface and the mean diameter is ca. 90 nm. The morphology and structure of $[YF_3:Eu^{3+}/PVP]//[PANI/Fe_3O_4/PVP]$ Janus nanofibers (sample S_2) were characterized by the combination of SEM and TEM. The mean diameter of the individual nanofiber of each Janus nanofiber is ca. 420 nm. As seen from Fig. 3c, d, the obtained products consist of two aligned nanofibers, which is composed of a dark-colored strand ($PANI/Fe_3O_4/PVP$) and a light-colored strand ($YF_3:Eu^{3+}/PVP$). Fe_3O_4 nanoparticles are only scattered in the dark-colored strand. Meanwhile, $YF_3:Eu^{3+}$ nanofibers are only dispersed in the light-colored strand, which confirms that the Janus nanofibers were successfully fabricated. The EDS analysis, as shown in Fig. 3e, reveals that the $[YF_3:Eu^{3+}/PVP]//[PANI/Fe_3O_4/PVP]$ Janus nanofibers are composed of C, N, O, Y, F, Eu, S and Fe elements, Au peak is from the conductive film of Au plated on the sample for SEM observation. The SEM image of YF_3: $Eu^{3+}/PANI/Fe_3O_4/PVP$ composite nanofibers is revealed in Fig. 3f, one can see that the composite nanofibers are relatively smooth and the mean diameter is ca. 300 nm.

3.3 Fluorescent performance

In order to investigate the impact of the mass percentage of PANI to PVP on the fluorescent performance, a series of

$[YF_3:Eu^{3+}/PVP]//[PANI/Fe_3O_4/PVP]$ Janus nanofibers were fabricated. For performing this study, the mass ratio of $YF_3:Eu^{3+}$ nanofibers to PVP was settled as 1:1, the mass ratios of Fe_3O_4 to PVP was fixed as 1:3 and the mass percentages of PANI to PVP were varied from 20 to 70 % (samples S_1, S_2, S_3, S_4). The Fig. 4a demonstrates the excitation spectra of the samples. The excitation spectrum is dominated by the $^7F_0 \rightarrow {}^5L_6$ transition of Eu^{3+} centering at about 395 nm. The position of other peaks is practically identical to the characteristic absorption bands for f–f transitions in trivalent europium [45]. The emission spectra of the samples are shown in Fig. 4b. The emission peaks at 587, 595, 614 and 622 nm are ascribed to the $^5D_0 \rightarrow {}^7F_1$, $^5D_0 \rightarrow {}^7F_1$, $^5D_0 \rightarrow {}^7F_2$ and $^5D_0 \rightarrow {}^7F_2$ energy levels transitions of Eu^{3+} ions, respectively. The $^5D_0 \rightarrow {}^7F_1$ transition is mainly magnetically allowed and is not dependent on the site symmetry at which europium is situated [46]. The $^5D_0 \rightarrow {}^7F_2$ is a forced electric-dipole transition being allowed only at low symmetries without inversion centers. If the Eu^{3+} ions would occupy the position with inversion symmetry, the $^5D_0 \rightarrow {}^7F_1$ emission peaks are expected to have the highest intensity due to their magnetic-dipole character. If the Eu^{3+} ions would occupy the position which is without inversion symmetry, the $^5D_0 \rightarrow {}^7F_2$ emission is expected to be dominant. The strongest emission peaks are centered at 587 and 595 nm, which are much stronger than those of the 614 and 622 nm emissions, indicating that Eu^{3+} occupies a site with inversion symmetry in the $YF_3:5 \%Eu^{3+}$ nanofibers.

It is found from Fig. 4a, b that both excitation and emission intensity of the Janus nanofibers are decreased with the increased of the amount of PANI introduced into the Janus nanofibers. This phenomenon can be considered by the light absorption of dark-colored PANI which were mixed into the nanofibers. From the absorbance spectrum of PANI/PVP nanofibers illustrated in Fig. 4c, it is observed that PANI/PVP nanofibers strongly absorb the light in the regions of 270–360, 380–450 and 500–800 nm. Thus, the exciting light (395 nm) and emitting light (587, 595, 614 and 622 nm) are absorbed by the $[PANI/Fe_3O_4/PVP]$ half side and the intensities are decreased, furthermore, the light absorption would become stronger with introducing more PANI into the dark-colored half side.

Meanwhile, the effect on fluorescence intensity via introducing different ratios of Fe_3O_4 NPs (samples S_2, S_5, S_6) into Janus nanofibers was also studied. As seen from Fig. 5a, b, the excitation and emission intensity of the $[YF_3:Eu^{3+}/PVP]//[PANI/Fe_3O_4/PVP]$ Janus nanofibers are decreased with the increase of the amount of Fe_3O_4 NPs. This phenomenon results from the light absorption of Fe_3O_4 NPs which are mixed into the nanofibers [47]. From the absorbance spectrum of Fe_3O_4 NPs illustrated in Fig. 5c, it is seen that the Fe_3O_4 NPs can absorb light at
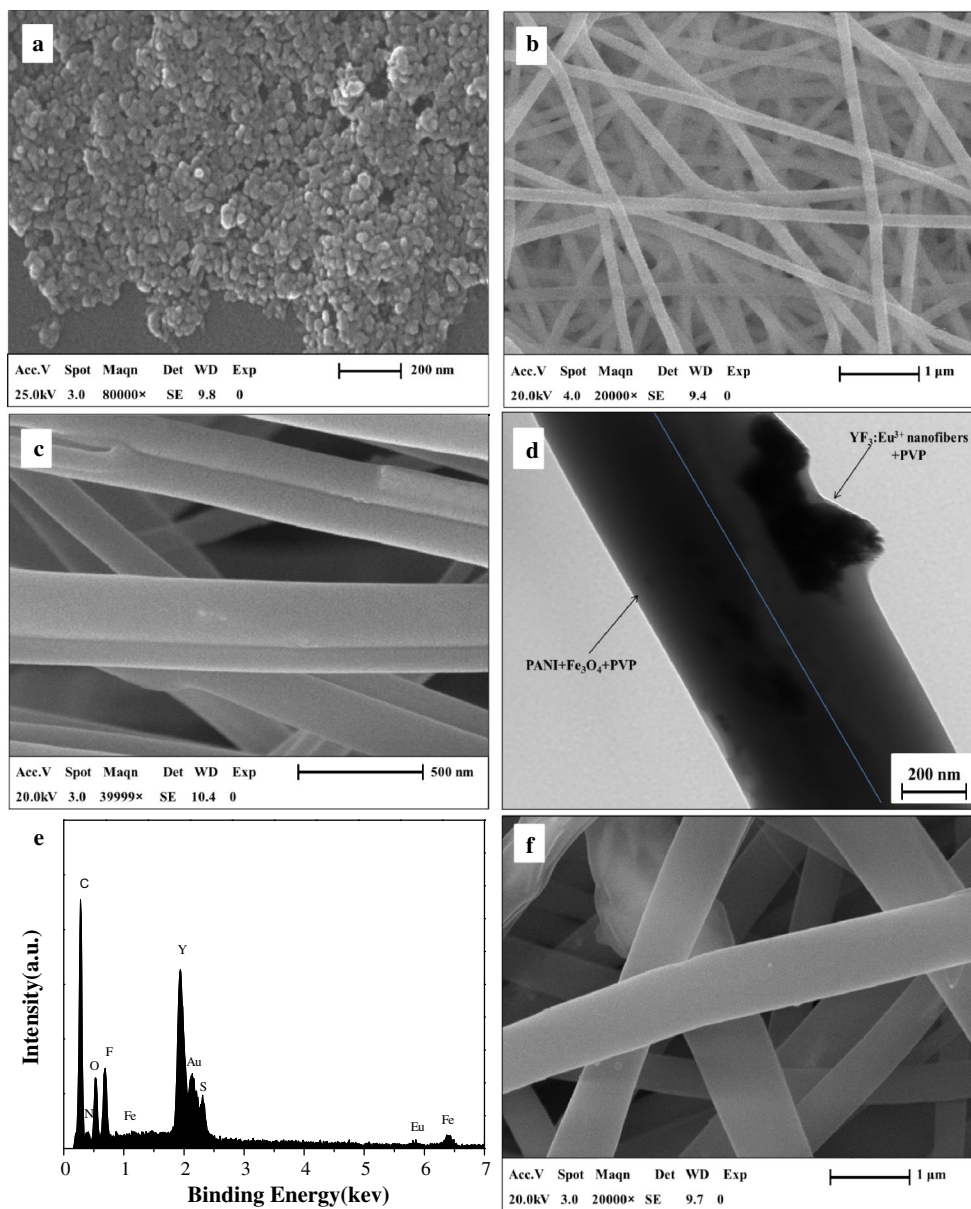
Fig. 3 SEM images of Fe_3O_4 nanoparticles (**a**), $YF_3:Eu^{3+}$ nanofibers (**b**), and SEM image (**c**), TEM image (**d**) and EDS spectrum (**e**) of $[YF_3:Eu^{3+}/PVP]//[PANI/Fe_3O_4/PVP]$ Janus nanofibers and SEM image of $YF_3:Eu^{3+}/PANI/Fe_3O_4/PVP$ composite nanofibers (**f**)

ultraviolet wavelength (<400 nm) much more strongly than visible range (400–700 nm). Thus, the exciting light (395 nm) and emitting light (587, 595, 614 and 622 nm) are absorbed by the strand $[PANI/Fe_3O_4/PVP]$ and the intensities are decreased, furthermore, the light absorption would become stronger with introducing more Fe_3O_4 nanoparticles into the Janus nanofibers.

The fluorescent properties of the $[YF_3:Eu^{3+}/PVP]//[PANI/Fe_3O_4/PVP]$ Janus nanofibers containing different ratios of $YF_3:Eu^{3+}$ nanofibers (samples S_2, S_7, S_8) were investigated. As shown in Fig. 6a, b. It can be seen that the excitation and emission intensity of Janus nanofibers are

increased with the increase of the amount of $YF_3:Eu^{3+}$ nanofibers.

The fluorescent properties of $[YF_3:Eu^{3+}/PVP]//[PANI/Fe_3O_4/PVP]$ Janus nanofibers (sample S_2) are further investigated by comparing with that of $YF_3:Eu^{3+}/PANI/Fe_3O_4/PVP$ composite nanofibers under the same components and contents of the two kinds of nanostructures. As manifested in Fig. 7, it is found that the fluorescence intensity of $[YF_3:Eu^{3+}/PVP]//[PANI/Fe_3O_4/PVP]$ Janus nanofibers is obviously higher than that of $YF_3:Eu^{3+}/PANI/Fe_3O_4/PVP$ composite nanofibers. This phenomenon can be explained by the strong light absorption of the
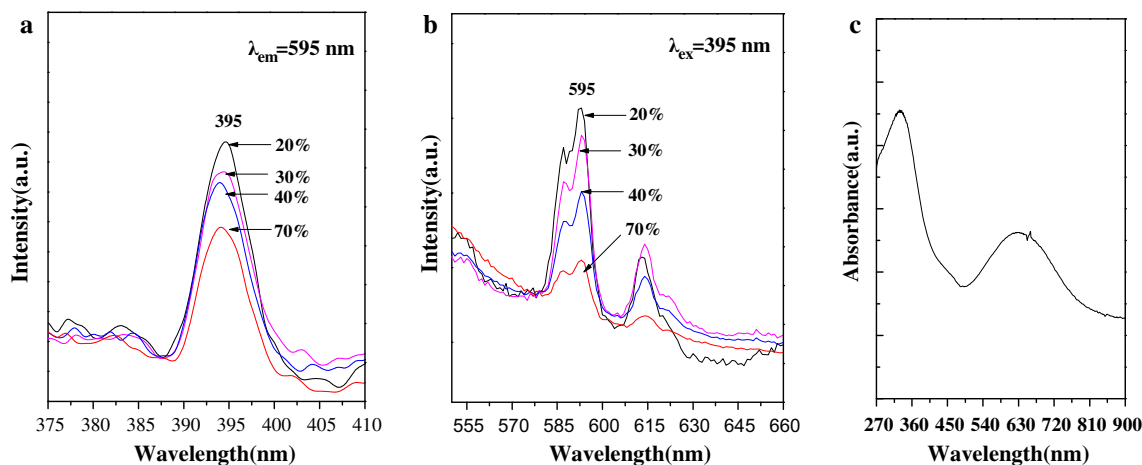
Fig. 4 Excitation spectra (**a**) and emission spectra (**b**) of [YF$_3$:Eu^{3+}/PVP]//[PANI/Fe$_3$O$_4$/PVP] Janus nanofibers containing different mass percentages of PANI when the mass ratios of Fe$_3$O$_4$ NPs to PVP was fixed to 1:3 and the mass percentage of YF$_3$:Eu^{3+} to PVP were fixed to 100 % and UV–Vis absorbance spectrum of PANI (**c**)
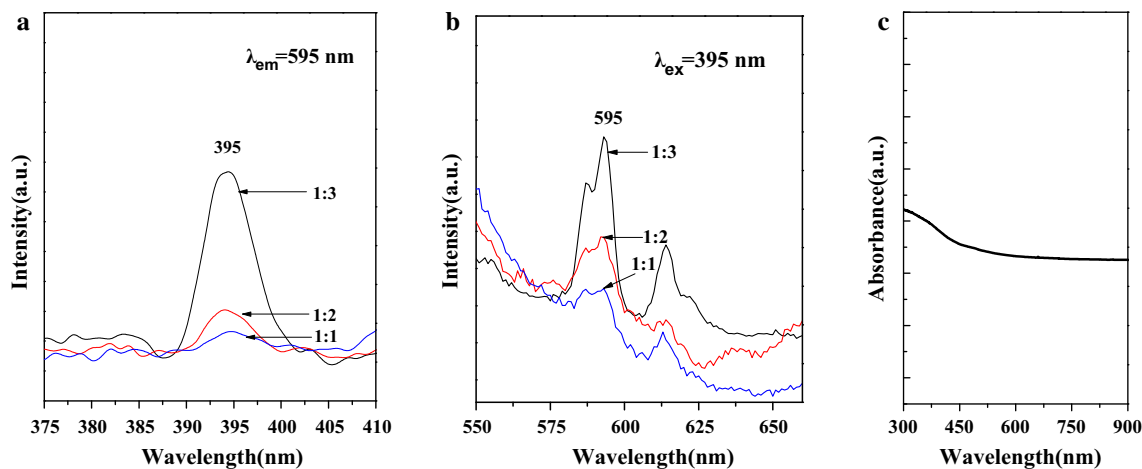

Fig. 5 Excitation spectra (**a**) and emission spectra (**b**) of [YF$_3$:Eu^{3+}/PVP]//[PANI/Fe$_3$O$_4$/PVP] Janus nanofibers containing different mass ratio of Fe$_3$O$_4$ NPs when the mass percentage of PANI to PVP was settled as 30 % and the mass percentage of YF$_3$:Eu^{3+} to PVP was fixed to 100 % and UV–Vis absorbance spectrum of Fe$_3$O$_4$ (**c**)

Fig. 6 Excitation spectra (**a**) and emission spectra (**b**) of [YF$_3$:Eu^{3+}/PVP]//[PANI/Fe$_3$O$_4$/PVP] Janus nanofibers containing different mass ratio of YF$_3$:Eu^{3+} nanofibers when the mass percentage of PANI to PVP was settled as 30 % and the mass percentage of Fe$_3$O$_4$ NPs to PVP was fixed to 1:3
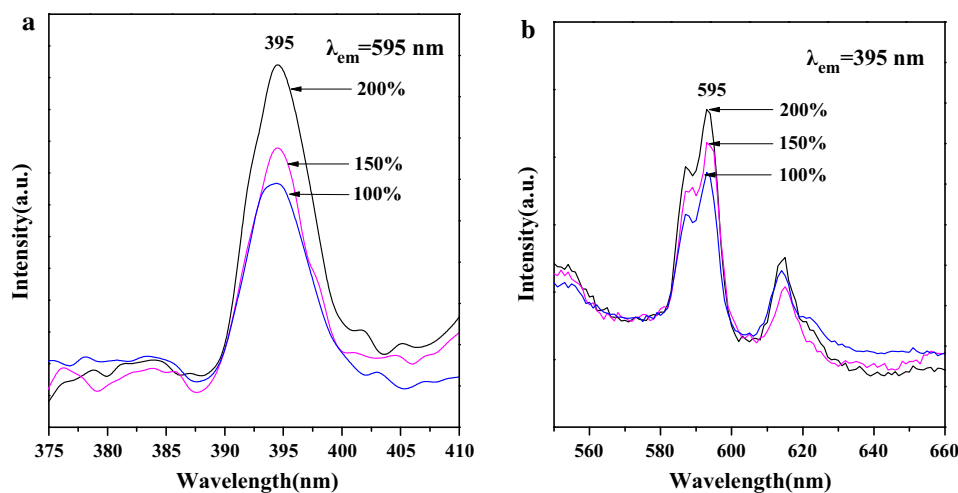
Fig. 7 Excitation spectra (**a**) and emission spectra (**b**) of [YF$_3$:Eu^{3+}/PVP]//[PANI/Fe$_3$O$_4$/PVP] Janus nanofibers and YF$_3$:Eu^{3+}/PANI/Fe$_3$O$_4$/PVP composite nanofibers
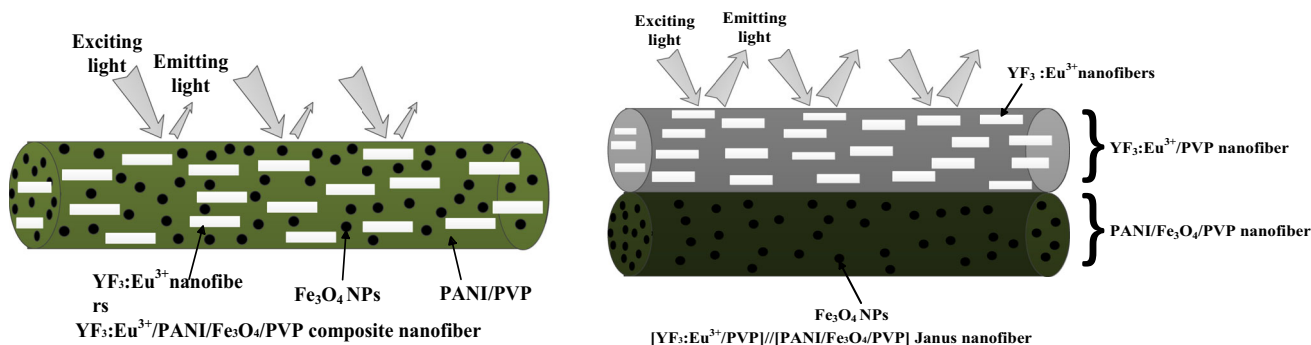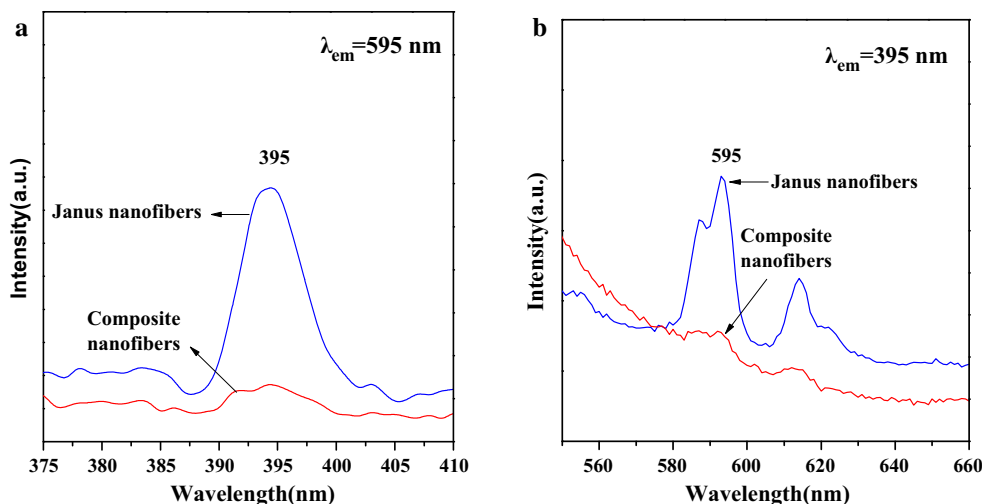
Fig. 8 Schematic diagrams of the exciting light and emitting light in YF$_3$:Eu^{3+}/PANI/Fe$_3$O$_4$/PVP composite nanofiber and [YF$_3$:Eu^{3+}/PVP]//[PANI/Fe$_3$O$_4$/PVP] Janus nanofiber

dark-colored PANI and Fe$_3$O$_4$ NPs when PANI, Fe$_3$O$_4$ NPs and YF$_3$:Eu^{3+} nanofibers are mixed together. As illustrated in Fig. 8, YF$_3$:Eu^{3+} nanofibers are directly distributed into the PANI/Fe$_3$O$_4$/PVP nanofiber, the exciting light has to pass through PANI and Fe$_3$O$_4$ NPs to reach the YF$_3$:Eu^{3+} nanofibers. In this process, a large part of the exciting light has been absorbed by the PANI and Fe$_3$O$_4$ NPs, and thus the exciting light is much weakened before it reaches the YF$_3$:Eu^{3+} nanofibers. Similarly, the emitting light emitted by the YF$_3$:Eu^{3+} nanofibers also has to pass through PANI and Fe$_3$O$_4$ NPs and is absorbed by them. Consequently, the exciting and emitting light are severely weakened. For [YF$_3$:Eu^{3+}/PVP]//[PANI/Fe$_3$O$_4$/PVP] Janus nanofiber, the PANI and Fe$_3$O$_4$ NPs are efficiently isolated from YF$_3$:Eu^{3+} nanofibers so that the exciting light and emitting light in the strand YF$_3$:Eu^{3+}/PVP will be little affected by the PANI and Fe$_3$O$_4$ NPs. The overall effect is that the [YF$_3$:Eu^{3+}/PVP]//[PANI/Fe$_3$O$_4$/PVP] Janus nanofiber possess much higher fluorescent performance than the YF$_3$:Eu^{3+}/PANI/Fe$_3$O$_4$/PVP composite nanofibers. Thus, Janus nanofibers possess strong fluorescent emission

intensity through isolating the YF$_3$:Eu^{3+} nanofibers from PANI and Fe$_3$O$_4$ NPs.

3.4 Electrical conductivity

The average electrical conductivity values of the samples are summarized in Table 2. It is found from Table 2 that the conductivity is greatly increased from 9.276×10^{-7} to 3.458×10^{-4} S cm^{-1} in the beginning when the PANI is incorporated into Janus nanofibers. When the concentration of PANI to PVP is 30 %, with further increase in PANI content, the conductivity of Janus nanofibers is only slightly changed. The increase in conductivity of [YF$_3$:Eu^{3+}/PVP]//[PANI/Fe$_3$O$_4$/PVP] Janus nanofibers with increasing in PANI content is due to forming a better continuous net structure for PANI polymer, which render more efficient charge transport. When the mass of Fe$_3$O$_4$ to PVP was changed from 1:3 to 1:1, it is found from Table 2 that the conductivity decreases with the increase of Fe$_3$O$_4$ in the Janus nanofibers owing to the fact that the polymerization of aniline is influenced by Fe$_3$O$_4$ naoparticles

Table 2 Electrical conductivity of the samples doped with various amount of PANI and Fe_3O_4

Samples	Conductivity (S cm^{-1})
Janus nanofibers [PANI:PVP = 20 %, S_1]	9.276×10^{-7}
Janus nanofibers [PANI:PVP = 30 %, S_2]	3.458×10^{-4}
Janus nanofibers [PANI:PVP = 40 %, S_3]	7.190×10^{-4}
Janus nanofibers [PANI:PVP = 70 %, S_4]	8.919×10^{-4}
Janus nanofibers [Fe_3O_4:PVP = 1:2, S_5]	8.861×10^{-5}
Janus nanofibers [Fe_3O_4:PVP = 1:1, S_6]	9.810×10^{-6}
Y_2O_3:Eu^{3+}/PANI/Fe_3O_4/PVP composite nanofibers	3.284×10^{-6}
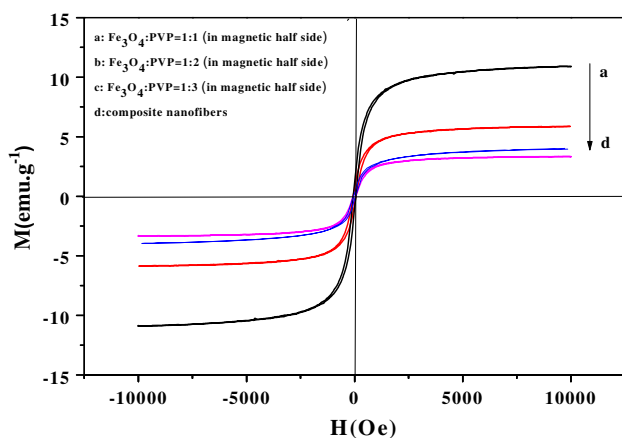
Fig. 9 Hysteresis loops of YF$_3$:Eu^{3+}/PANI/Fe_3O_4/PVP composite nanofibers and [YF$_3$:Eu^{3+}/PVP]//[PANI/Fe_3O_4/PVP] Janus nanofibers

Table 3 Saturation magnetization of [YF$_3$:Eu^{3+}/PVP]//[PANI/Fe_3O_4/PVP] Janus nanofiber and YF$_3$:Eu^{3+}/PANI/Fe_3O_4/PVP composite nanofibers

Samples	Ms (emu g^{-1})
Janus nanofibers, Fe_3O_4:PVP = 1:1 (in magnetic half)	10.89
Janus nanofibers, Fe_3O_4:PVP = 1:2 (in magnetic half)	5.85
Janus nanofibers, Fe_3O_4:PVP = 1:3 (in magnetic half)	3.96
YF$_3$:Eu^{3+}/PANI/Fe_3O_4/PVP composite nanofibers	3.33

[48]. The conductivities of Janus nanofibers can be tuned by adjusting the mass ratios of PANI to PVP and Fe_3O_4 to PVP.

It can be apparently found that the conductivity of the YF$_3$:Eu^{3+}/PANI/Fe_3O_4/PVP composite nanofibers is lower than that of Janus nanofibers. The decrease of the conductivity is mainly due to the addition of non-conducting Fe_3O_4 nanoparticles, PVP and YF$_3$:Eu^{3+} nanofibers that decreases the conducting PANI content of the YF$_3$:Eu^{3+}/PANI/Fe_3O_4/PVP composite nanofibers and partially hinders the formation of conductive paths [49].

3.5 Magnetic property

The typical hysteresis loops for YF$_3$:Eu^{3+}/PANI/Fe_3O_4/PVP composite nanofibers and [YF$_3$:Eu^{3+}/PVP]//[PANI/Fe_3O_4/PVP] Janus nanofibers containing various mass ratios of Fe_3O_4 NPs are indicated in Fig. 9, and their saturation magnetizations are listed in Table 3. It is well known that the saturation magnetization of a magnetic composite material depends on the mass percentage of the magnetic substance in the magnetic composite material. It is found that the saturation magnetization of the Janus nanofibers is increased from 3.96 to 10.89 emu g^{-1} with the increase of Fe_3O_4 NPs, which indicates that the

magnetic properties of the Janus nanofibers can be tuned via addition of various amounts of Fe_3O_4 NPs. Besides, the saturation magnetization of the YF$_3$:Eu^{3+}/PANI/Fe_3O_4/PVP composite nanofibers is 3.33 emu g^{-1} which is close to that of the Janus nanofibers (3.97 emu g^{-1}) because they were both prepared under the same conditions except for the spinneret. Analyses from combining the fluorescent performance with the electrical conductivity, one can see that the [YF$_3$:Eu^{3+}/PVP]//[PANI/Fe_3O_4/PVP] Janus nanofibers have the close magnetic property compared with YF$_3$:Eu^{3+}/PANI/Fe_3O_4/PVP composite nanofibers, but the electrical conductivity and the fluorescent intensity of [YF$_3$:Eu^{3+}/PVP]//[PANI/Fe_3O_4/PVP] Janus nanofibers are much higher than those of YF$_3$:Eu^{3+}/PANI/Fe_3O_4/PVP composite nanofibers, and this further demonstrates that the Janus nanofibers have better luminescent–electrical–magnetic performance than the counterpart composite nanofibers. Based on the above experimental results, we can safely conclude that those academic ideas described in the introduction can be successfully realized via specially designed parallel spinnerets electrospinning.

4 Conclusions

In summary, novel [YF$_3$:Eu^{3+}/PVP]//[PANI/Fe_3O_4/PVP] luminescent–electrical–magnetic trifunctional Janus nanofibers were successfully prepared by a simple electrospinning process using a side-by-side dual spinneret. One half side of the Janus nanofibers is composed of PANI, Fe_3O_4 NPs and PVP, and the other half side consists of

YF$_3$:Eu^{3+} nanofibers and PVP. Compared to composite nanofibers, it is very gratifying to see that the Janus nanofibers possess higher fluorescent intensity, saturation magnetization and conductivity. In addition, the luminescent intensity, electrical conductivity and magnetic properties of the Janus nanofibers can be tunable by adjusting the content of YF$_3$:Eu^{3+}, PANI and Fe$_3$O$_4$ NPs, respectively. The Janus nanofibers have potential applications in many fields such as electromagnetic interference shielding, microwave absorption, molecular electronics and biomedicine due to their excellent conduction, magnetism and fluorescence performance.

References

1. Q.L. Ma, W.S. Yu, X.T. Dong, J.X. Wang, G.X. Liu, Nanoscale **6**, 2945–2952 (2014)
2. Q.L. Ma, J.X. Wang, X.T. Dong, W.S. Yu, G.X. Liu, ChemPlusChem **79**, 290–297 (2014)
3. X. Xi, J.X. Wang, X.T. Dong, Q.L. Ma, W.S. Yu, G.X. Liu, Chem. Eng. J. **254**, 259–267 (2014)
4. N. Lv, Q.L. Ma, X.T. Dong, J.X. Wang, W.S. Yu, G.X. Liu, ChemPlusChem **79**, 690–697 (2014)
5. W.W. Ma, W.S. Yu, X.T. Dong, J.X. Wang, G.X. Liu, Chem. Eng. J. **244**, 531–539 (2014)
6. W.W. Ma, X.T. Dong, J.X. Wang, W.S. Yu, G.X. Liu, J. Mater. Sci. Mater. Electron. **25**, 1657–1663 (2014)
7. W.S. Yu, Q.L. Kong, J.X. Wang, X.T. Dong, G.X. Liu, J. Mater. Sci. Mater. Electron. **25**, 46–56 (2014)
8. S. Wu, X.T. Dong, J.X. Wang, Q.L. Kong, W.S. Yu, G.X. Liu, J. Mater. Sci. Mater. Electron. **25**, 1053–1062 (2014)
9. S.J. Sheng, Q.L. Ma, X.T. Dong, N. Lv, J.X. Wang, W.S. Yu, G.X. Liu, J. Mater. Sci. Mater. Electron. **25**, 2279–2286 (2014)
10. W. Sambaer, M. Zatloukal, D. Kimmer, Chem. Eng. Sci. **66**, 613–623 (2011)
11. X.H. Li, C.L. Shao, Y.C. Liu, X.T. Zhang, S.K. Hark, Mater. Lett. **62**, 2088–2091 (2008)
12. J.M. Corres, Y.R. Garcia, F.J. Arregui, I.R. Matias, IEEE Sens. J. **11**, 2383–2387 (2011)
13. S.L. Chen, H.Q. Hou, F. Harnisch, S.A. Patil, A.A. Carmona-Martinez, S. Agarwal, Y.Y. Zhang, S. Sinha-Ray, A.L. Yarin, A. Greiner, U. Schröder, Energy Environ. Sci. **4**, 1417–1421 (2011)
14. X.F. Lu, C. Wang, Y. Wei, Small **5**, 2349–2370 (2009)
15. P.-I. Gouma, US Patent 20070272901, 29 Nov (2007)
16. M. Stein, J. Wieland, P. Steurer, F. Tölle, R. Mülhaupt, B. Breit, Adv. Synth. Catal. **353**, 523–527 (2011)
17. H. Tan, J.M. Xue, B. Shuter, X. Li, J. Wang, Adv. Funct. Mater. **20**, 722–731 (2010)
18. S.L. Zhong, Y.H. Lu, Z.Z. Huang, S.P. Wang, J.J. Chen, Opt. Mater. **32**, 966–970 (2010)
19. H.Y. Li, C.M. Chang, K.Y. Hsu, Y.L. Liu, J. Mater. Chem. **22**, 4855–4860 (2012)
20. Q.L. Ma, J.X. Wang, X.T. Dong, W.S. Yu, G.X. Liu, J. Xu, Opt. Mater. **35**, 526–530 (2013)
21. Y. Chen, H.R. Chen, S.J. Zhang, F. Chen, L.X. Zhang, J.M. Zhang, M. Zhu, H.X. Wu, L.M. Guo, J.W. Feng, J.L. Shi, Adv. Funct. Mater. **21**, 270–278 (2011)
22. K. Li, D. Ding, D. Huo, K.Y. Pu, N.N.P. Thao, Y. Hu, Z. Li, B. Liu, Adv. Funct. Mater. **22**, 3107–3115 (2012)
23. Q.L. Ma, J.X. Wang, X.T. Dong, W.S. Yu, G.X. Liu, J. Xu, J. Mater. Chem. **22**, 14438–14442 (2012)
24. G.Q. Gai, L.Y. Wang, X.T. Dong, C.M. Zheng, W.S. Yu, J.X. Wang, X.F. Xiao, J. Nanopart. Res. **15**, 1539–1547 (2013)
25. J.P. Lellouche, G. Senthil, A. Joseph, L. Buzhansky, I. Bruce, E.R. Bauminger, J. Schlesinger, J. Am. Chem. Soc. **127**, 11998–12006 (2005)
26. Z.M. Zhang, M.X. Wan, Y. Wei, Nanotechnology **16**, 2827–2832 (2005)
27. S.C. Wuang, K.G. Neoh, E.T. Kang, D.W. Pack, D.E. Leckband, J. Mater. Chem. **17**, 3354–3362 (2007)
28. J.R. Meng, C.Y. Shi, B.W. Wei, W.J. Yu, C.H. Deng, X.M. Zhang, J. Chromatogr. A **1218**, 2841–2847 (2011)
29. C.L. Yu, J. Zhai, Z. Li, M.X. Wan, M.Y. Gao, L. Jiang, Thin Solid Films **516**, 5107–5110 (2008)
30. Z.M. Zhang, M.X. Wan, Synth. Met. **132**, 205–212 (2003)
31. J.G. Deng, C.L. He, Y.X. Peng, J.H. Wang, X.P. Long, P. Li, A.S.C. Chan, Synth. Met. **139**, 295–301 (2003)
32. S.H. Xuan, Y.X.J. Wang, K.C.F. Leung, K.Y. Shu, J. Phys. Chem. C **112**, 18804–18809 (2008)
33. H.G. Wang, Y.X. Li, L. Sun, Y.C. Li, W. Wang, S. Wang, S.F. Xu, Q.B. Yang, J. Colloid Interface Sci. **350**, 396–401 (2010)
34. Q.L. Ma, W.S. Yu, X.T. Dong, J.X. Wang, G.X. Liu, J. Xu, J. Nanopart. Res. **14**, 1203–1209 (2012)
35. Y.H. Wang, J.X. Wang, X.T. Dong, W.S. Yu, G.X. Liu, Chem. J. Chin. Univ. **33**, 1657–1662 (2012)
36. Y.H. Wang, J.X. Wang, X.T. Dong, W.S. Yu, G.X. Liu, Acta Chim. Sinica **70**, 1576–1582 (2012)
37. I. Salib, X. Yong, E.J. Crabb, N.M. Moellers, G.T. McFarlin IV, O. Kuksenok, A.C. Balazs, ACS Nano **7**, 1224–1238 (2013)
38. Q.L. Ma, J.X. Wang, X.T. Dong, W.S. Yu, G.X. Liu, Chem. Eng. J. **222**, 16–22 (2013)
39. M.M. Moghani, B. Khomami, Soft Matter **9**, 4815–4821 (2013)
40. C. Song, X.T. Dong, Optoelectron. Adv. Mater.-Rapid Commun. **6**, 319–323 (2012)
41. N.K. Reddy, L.J. Palangetic, L. Stappers, J. Buitenhuis, J. Fransaer, C. Clasen, J. Mater. Chem. C **1**, 3646–3650 (2013)
42. N.K. Reddy, C. Clasen, Korea-Aust. Rheol. J. **26**, 73–79 (2014)
43. D.S. Justin, S.A. Jennifer, Chem. Commun. **49**, 4151–4153 (2013)
44. Y. Hou, X.T. Dong, J.X. Wang, G.X. Liu, L.H. Li, Chem. J. Chin. Univ. **32**, 225–230 (2011)
45. H. Zhang, H.F. Li, D.Q. Li, S.L. Meng, J. Colloid Interface Sci. **302**, 509–515 (2006)
46. M. Ogawa, Y. Ide, M. Mizushima, Chem. Commun. **46**, 2241–2243 (2010)
47. Q. Gao, G.Y. Hong, J.Z. Ni, W.D. Wang, J.K. Tang, J.B. He, J. Magn. Magn. Mater. **321**, 1052–1057 (2009)
48. Z.M. Zhang, Q. Li, L.M. Yu, Z.J. Cui, L.J. Zhang, G.A. Bowmaker, Macromolecules **44**, 4610–4615 (2011)
49. G.H. Qiu, Q. Wang, M. Nie, J. Appl. Polym. Sci. **102**, 2107–2111 (2006)